

# CHEBYSHEV COLLOCATION METHOD AND MULTIDOMAIN DECOMPOSITION FOR THE INCOMPRESSIBLE NAVIER-STOKES EQUATIONS

A. PINELLI AND A. VACCA\*

*Von Karman Institute for Fluid Dynamics, Chaussée de Waterloo 72, B-1640 Rhode-St.-Genèse, Belgium*

## SUMMARY

The two-dimensional incompressible Navier–Stokes equations in primitive variables have been solved by a pseudospectral Chebyshev method using a semi-implicit fractional step scheme. The latter has been adapted to the particular features of spectral collocation methods to develop the monodomain algorithm. In particular, pressure and velocity collocated on the same nodes are sought in a polynomial space of the same order; the cascade of scalar elliptic problems arising after the spatial collocation is solved using finite difference preconditioning. With the present procedure spurious pressure modes do not pollute the pressure field.

As a natural development of the present work a multidomain extent was devised and tested. The original domain is divided into a union of patching sub-rectangles. Each scalar problem obtained after spatial collocation is solved by iterating by subdomains. For steady problems a  $C^1$  solution is recovered at the interfaces upon convergence, ensuring a spectrally accurate solution.

A number of test cases have been solved to validate the algorithm in both its single-block and multidomain configurations.

The preliminary results achieved indicate that collocation methods in multidomain configurations might become a viable alternative to the spectral element technique for accurate flow prediction.

KEY WORDS Incompressible Navier–Stokes Collocated Chebyshev schemes Domain decomposition

## 1. INTRODUCTION

Various spectral methods are currently being developed and used in computational fluid dynamics. Their major advantage is the high accuracy attained by the resulting discretization for a given number of nodes or, conversely, the saving in computational resources for a given accuracy. The difficulty in applying such methods to real-life problems arises when the geometry to be considered departs from a simple rectangle, as first emphasized by Orzag.<sup>1</sup>

In the past decade intensive research has been devoted to overcoming this apparent limitation. The present cure technique may be divided into two categories, although combinations of both are effectively used. On one hand, domain decomposition methods allow the partitioning of the global geometry into elementary quadrangles. Active investigation still goes on in this field, as underlined by the numerous contributions to dedicated symposia.<sup>2,3</sup> On the other hand, suitable co-ordinate transformations are created in order to map the arbitrary physical domain into the reference square space where the polynomial bases as interpolants are

---

\* Present address: Dipartimento di Ingegneria Idraulica, Università degli Studi di Napoli Federico II, Via Claudio 21, I-80125 Napoli, Italy.

defined. For 2D computations such transformation methods take on different forms—algebraic, interpolation, conformal mapping or solution of differential equations—adding up to a widespread field as surveyed e.g. by Eisemann and Erlebacher.<sup>4</sup> Some spectral practitioners have proposed their own technique to cope with non-rectangular geometries. In the case of numerical solution of the Navier–Stokes equations Patera<sup>5</sup> developed the spectral element method which combines mapping with a domain decomposition strategy.<sup>6</sup> Curvilinear subdomains were incorporated by Metivet<sup>7</sup> into a Schwarz domain decomposition algorithm applied to a spectral collocation method.

In the same framework we present a Chebyshev collocated multidomain algorithm for the solution of the incompressible Navier–Stokes equations in their primitive variable formulation.

First we introduce and validate the single-block solver and later we illustrate the multidomain strategy that has been developed and tested.

For the single-block solver we have selected the ‘pressure correction’ scheme of Van Kan.<sup>8</sup> The latter is a second-order-in-time ‘semi-implicit’ scheme belonging to the family of projection (i.e. fractional step) methods. A typical feature of the present implementation lies in the preconditioned iterative methods adopted for the inversion of the two Helmholtz problems for the predicted velocity field (arising when the viscous terms are treated implicitly) and of the Poisson equation for the pressure.

A single grid was used for treating both pressure and velocity. Spurious pressure modes do not appear because they are implicitly filtered out by the solution process adopted for the inversion of the pseudospectral Laplace operator associated with the Poisson problem. The main features of the present algorithm satisfy some of the more desirable properties one tries to achieve when setting up a computational kernel to be used in a multidomain solver:

- (i) high spectral accuracy
- (ii) no spurious modes except the physical one (constant solution)
- (iii) no staggered grids.

To validate the algorithm, a series of test cases have been solved, including (i) a driven flow in a regularized square cavity for a Reynolds number  $Re$  as high as 10,000 and (ii) a thermally driven cavity in two different configurations (using the Boussinesq approximation). The capability of the developed code in dealing with unsteady flows has been tested by solving the regularized driven cavity at  $Re = 10,500$ , where the flow motion is no longer steady.

Having set up a quite effective single-block algorithm, we turned our attention to the development of a multidomain solver having as a computational kernel the monodomain one. On the practical side we took advantage of the typical features of the monodomain algorithm: roughly speaking, the solution of the Navier–Stokes equations is achieved by inverting at each time step three elliptic scalar problems (i.e. one for the  $x$ -component of velocity, one for the  $y$ -component of velocity and the last one for the pressure). For each scalar problem a well-established technique (‘iteration by subdomains’ as proposed by Funaro *et al.*<sup>9</sup>) was introduced to solve each scalar equation on the original domain split into a union of non-overlapping squares.

The present paper arranged as follows. After a general overview we present the developed single-block algorithm together with the test cases that have been used for its validation. Later on we illustrate the multidomain technique and the validation that has been carried out to demonstrate the viability of the proposed algorithm.

## 2. BASIC EQUATIONS

We consider here the incompressible Navier–Stokes equations in the primitive variables formulation  $(\mathbf{u}, p)$  with the non-linear terms expressed in a skew-symmetric form to minimize aliasing effects:

$$\partial \mathbf{u} / \partial t = -\nabla p + \nu \Delta \mathbf{u} - \frac{1}{2}[\mathbf{u} \cdot \nabla \mathbf{u} + \nabla \cdot (\mathbf{u}\mathbf{u})], \quad (1)$$

$$\nabla \cdot \mathbf{u} = 0, \quad (2)$$

where  $\mathbf{u}$  is the velocity field,  $p$  is the pressure and  $\nu = \mu/\rho$  is the kinematic viscosity ( $\rho$  is constant). The pressure in the given set of equations (1), (2) is not a thermodynamic variable satisfying an equation of state, but is instead a dynamic variable which adjusts itself instantaneously in a time-dependent flow to satisfy the incompressibility constraint (2).

Most existing algorithms of the spectral type deal with the Navier–Stokes equations in the primitive variable formulation  $(\mathbf{u}, p)$ . In this case velocity and pressure cannot be approximated independently: a compatibility condition must be satisfied by the finite-dimensional spaces in which velocity and pressure are sought in order to have a solvable system<sup>10</sup> leading to a pressure field not polluted by spurious pressure wiggles.

Spurious pressure modes for the two-dimensional case are restricted to the set  $Z_N$  of all polynomials in  $P_N \otimes P_N$  (space of polynomials of degree  $N$ ) defined as

$$Z_N = \text{span}\{1, p_N(x), p_N(y), p_N(x)p_N(y), p'_{N+1}(x)p'_{N+1}(y), p'_N(x)p'_{N+1}(y), p'_{N+1}(x)p'_N(y), p'_N(x)p'_N(y)\}, \quad (3)$$

where  $p_N$  is the  $N$ th mode ( $p_{N+1}$  is the  $N+1$ th) and  $p'_N$  is the first derivative of the  $N$ th mode ( $p'_{N+1}$  is the first derivative of the  $N+1$ th). Apart from the physical constant mode,  $Z_N$  is made of polynomials that are of degree  $N$  and  $N-1$ . The fact that the spurious modes are characterized only by high frequencies is a relevant point of which we will make use in the following.

In the next subsection the projection schemes are introduced and attention is focused on the algorithm that we have selected, modified and tested in the present work.

### 2.1. Semidiscretized equations

In the incompressible Navier–Stokes equations the velocity and pressure are coupled together by the incompressibility condition, which makes the equations difficult to solve. Classical procedures to overcome this drawback are provided by time-splitting schemes.

This class of numerical methods was originally devised for the incompressible Navier–Stokes equations by Chorin and Marsden<sup>12</sup> and Temam.<sup>13</sup> The basic idea is to decouple the pressure and velocity computations at each time step. The terms associated with the spatial derivatives appearing in the given equations might be computed at an old, a new or some intermediate time step. Implicit treatment of the viscous terms allows one to overcome the most severe time step restriction met when dealing with spectral collocation methods:

$$\Delta t \sim Re \frac{1}{N^4} \quad (Re, \text{ Reynolds number}). \quad (4)$$

For the present work we selected the ‘pressure correction scheme’ developed by Van Kan:<sup>8</sup>

$$\frac{\hat{\mathbf{u}} - \mathbf{u}^n}{\Delta t} - \frac{\nu}{2} \Delta(\hat{\mathbf{u}} + \mathbf{u}^n) + \nabla p^n = -\frac{3}{2}(\mathbf{u}^n \cdot \nabla)\mathbf{u}^n + \frac{1}{2}(\mathbf{u}^{n-1} \cdot \nabla)\mathbf{u}^{n-1}, \quad (5)$$

$$\hat{\mathbf{u}}_{\partial\Omega} = \mathbf{u}[(n+1)\Delta t], \quad (6)$$

$$\frac{\mathbf{u}^{n+1} - \hat{\mathbf{u}}}{\Delta t} + \frac{1}{2}\nabla(p^{n+1} - p^n) = 0, \quad (7)$$

$$\nabla \cdot \mathbf{u}^{n+1} = 0. \quad (8)$$

In the first step we solve an intermediate velocity field  $\hat{\mathbf{u}}$  which is not physical. In fact,  $\hat{\mathbf{u}}$  does not satisfy the incompressibility condition. Then in the second step we project  $\hat{\mathbf{u}}$  onto the divergence-free space to get an adequate velocity approximation  $\mathbf{u}^{n+1}$ .

The scheme with the given boundary conditions is nothing other than a second-order Crank–Nicolson Adams–Bashforth scheme with an  $\mathcal{O}(\Delta t^2)$  deviation in the tangent direction to the boundary:

$$\mathbf{u}^{n+1} \cdot \boldsymbol{\tau}|_{\partial\Omega} = \mathbf{u}[(n+1)\Delta t] \cdot \boldsymbol{\tau} - \frac{\Delta t}{2} \nabla(p^{n+1} - p^n) \cdot \boldsymbol{\tau}. \quad (9)$$

By applying the divergence operator to (7), we find that the latter is equivalent to

$$\Delta(p^{n+1} - p^n) = \frac{2}{\Delta t} \nabla \cdot \hat{\mathbf{u}}, \quad (10)$$

$$\left. \frac{\partial p^{n+1}}{\partial \mathbf{n}} \right|_{\partial\Omega} = 0, \quad (11)$$

$$\mathbf{u}^{n+1} = \hat{\mathbf{u}} - \frac{\Delta t}{2} \nabla(p^{n+1} - p^n). \quad (12)$$

At each time step we have to solve a cascade of scalar boundary value problems: two Helmholtz equations for the predicted value of velocity and a Poisson equation for the pressure. Having treated the diffusive part implicitly, the only stability restriction on the time step is given by the Courant (CFL) condition

$$\Delta t \sim \frac{1}{U} \frac{1}{N^2} \quad (U, \text{ maximum velocity}), \quad (13)$$

which is less severe, at least for low Reynolds number, than the one related to the viscous terms (4)

## 2.2. Space discretization

The unknowns in the pseudospectral method (strong collocation) are expanded as products of orthogonal polynomials,

$$g = \sum_{n=0}^N \sum_{m=0}^M g_{mn} T_n(x) T_m(y), \quad (14)$$

if Chebyshev polynomials  $T_n(x)$ ,

$$T_k(x) = \cos(k \cos^{-1} x), \quad (15)$$

have been used. The differential equations are satisfied at a particular set of collocation points,

$$x_j = \cos\left(\frac{\pi j}{N}\right), \quad j = 0, 1, \dots, N \quad (16)$$

and boundary conditions are enforced to determine the unknown coefficients  $g_{mn}$ . As mentioned in the previous subsection, collocation of (5) and (10) for a two-dimensional problem, here expressed in 'δ-form', translates into a cascade of three linear systems of equations to be inverted at each time step:

$$\left(\frac{1}{\Delta t} \mathbf{I} + \frac{\nu}{2} \mathcal{L}\right) \delta \hat{u}_i = \text{RHS}_i + \nu \mathcal{L} u_i^n, \quad i = 1, 2, \quad (17)$$

$$\mathcal{L} \delta p = -\frac{2}{\Delta t} \mathcal{D} \hat{u}, \quad (18)$$

where  $\mathcal{L}$  and  $\mathcal{D}$  represent the pseudospectral Laplace operator and the pseudospectral divergence operator respectively, and  $\text{RHS}_i$  is given by

$$\begin{aligned} \text{RHS}_i = & -\frac{3}{4} \left( u_i^n \frac{\partial u_i^n}{\partial x_i} + u_j^n \frac{\partial u_i^n}{\partial x_j} + \frac{\partial u_i^n u_i^n}{\partial x_i} + \frac{\partial u_i^n u_j^n}{\partial x_j} \right) \\ & + \frac{1}{4} \left( u_i^{n-1} \frac{\partial u_i^{n-1}}{\partial x_i} + u_j^{n-1} \frac{\partial u_i^{n-1}}{\partial x_j} + \frac{\partial u_i^{n-1} u_i^{n-1}}{\partial x_i} + \frac{\partial u_i^{n-1} u_j^{n-1}}{\partial x_j} \right), \end{aligned} \quad (19)$$

the advective part having been treated with a skew-symmetric formulation.<sup>14</sup> System (17) or (18) might be rewritten in compact notation as

$$\mathbf{L}U = F, \quad (20)$$

where  $\mathbf{L}$  is the matrix representing the pseudospectral approximation to either equation (17) or (18),  $U$  is the solution vector and  $F$  is the source term.

It is well known that system (20) is ill conditioned,<sup>15</sup> which rules out standard iterative methods for its solution (Gauss-Seidel-type methods). Moreover, the matrix  $\mathbf{L}$  is full and non-symmetric, which makes the use of direct methods for the inversion of the above system unattractive.<sup>15</sup> For the same reason it would also be extremely expensive to apply an iterative solution procedure directly to the linear set of equations (20). However, these difficulties can be overcome by introducing a preconditioning matrix  $\mathbf{H}^{-1}$  and rewriting (20) as

$$\mathbf{H}^{-1} \mathbf{L}U = \mathbf{H}^{-1} F. \quad (21)$$

If the inverse to  $\mathbf{H}$  is a good approximation of  $\mathbf{L}^{-1}$ , it is expected to obtain a new system matrix  $\mathbf{H}^{-1} \mathbf{L}$  which is very well conditioned. If this can be achieved, even a very simple iterative method such as the Richardson one,

$$V^{n+1} = V^n + \omega \mathbf{H}^{-1} (f - \mathbf{L}V^n), \quad (22)$$

will perform satisfactorily. Since equation (22) is solved by inverting at each iteration the system

$$\mathbf{H}(V^{n+1} - V^n) = \omega(f - \mathbf{L}V^n), \quad (23)$$

the matrix  $\mathbf{H}$  must evidently be much easier to invert than the matrix  $\mathbf{L}$  for the preconditioner to be cost-effective.

Preconditioning techniques have been investigated extensively using both finite difference and finite element methods to discretize the left-hand side of (23).<sup>15</sup> In particular, for a Chebyshev pseudospectral Laplace operator with Dirichlet boundary conditions, it can be shown that a second-order finite difference preconditioner, built on the collocation grid, bounds the eigenvalues of the matrix  $\mathbf{H}^{-1}\mathbf{L}$  in the range  $[1, \pi^2/4]$  (moreover, all the eigenvalues have no imaginary part), independently of the number of nodes used for the discretization.<sup>16</sup> When a Neumann problem is considered, the preconditioned eigenvalue spectrum is still bounded independently of the number of nodes if a one-sided first-order finite difference discretization is used to precondition the first-order operator at the boundary.<sup>15</sup> Although a good preconditioner guarantees fast convergence even for a simple Richardson method, the procedure for the iterative inversion of problem (20) can be accelerated by using a conjugate-gradient-like method.<sup>17</sup> Unfortunately, this family of methods cannot be applied in a straightforward way to pseudospectral discretizations which always produce non-symmetric matrices (only for Fourier approximations of self-adjoint problems will the collocation operators be symmetric). In our case it is necessary to select a method from the family of generalized conjugate residuals. This class of methods restores the orthogonality property of the direction vectors at the cost of a considerable increase in storage. A preconditioned version of the generalized conjugate residuals (GPCR) was selected for the solution of the present system.<sup>18</sup> The major drawback of such an algorithm lies in the considerable increase in both storage and operation count with respect to the standard Richardson algorithm. The price can be partially reduced if the convergence parameters are determined using only the last  $k$  iterations, which often can be done without reducing the rate of convergence too much. We found that very few restarts ( $\kappa \sim 3-5$ ) are sufficient to guarantee an effective speed-up ( $\sim 2$ ) with respect to the standard Richardson algorithm. Some more efficiency has been gained by 'LU decomposing' the finite difference preconditioner only once in a preprocessing stage.

### 2.3. Pressure treatment

As already mentioned, the pressure and velocity must fulfil a compatibility condition<sup>19</sup> to ensure a unique solution for the pressure. In the present work we discretized the pressure and velocity by using the same polynomial basis and collocating both on the same nodes (i.e. no staggered grid). Even if under such a condition spurious modes (3) should arise, we will show that our algorithm behaves like a 'low-bandpass' filter able to remove the spurious pressure modes.

A heuristic explanation might be introduced by considering a simple 1D model problem

$$\partial u / \partial t - \nu \partial^2 u / \partial x^2 + \partial p / \partial x = f(x), \quad (24)$$

$$\partial u / \partial x = 0. \quad (25)$$

If we select a Chebyshev collocated scheme to discretize (24), (25), we face only one spurious pressure mode  $T'_N(x)$  (apart from the constant mode). In fact, since the zeros of  $T'_N(x)$  are the Chebyshev-Gauss-Lobatto points,<sup>15</sup> such a mode is identically equal to zero on the collocation nodes. In other words, if  $(u(x), p(x))$  satisfies the system (24), (25), then  $(u(x), p(x) + T'_N(x))$  also satisfies the same set of equations.

We now consider a projection method (i.e. the Van Kan scheme) whereby the Poisson problem is solved by an iterative procedure preconditioned by a finite difference matrix discretizing the

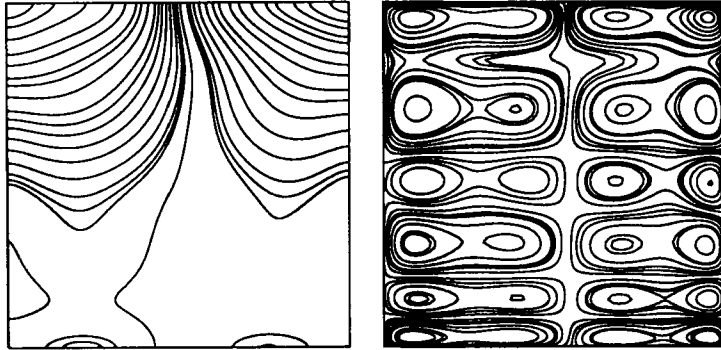


Figure 1. Filtered pressure field (left) and unfiltered pressure field (right)

same differential operator and constructed on the same support (i.e. on the same collocation nodes). In this case the solution is built as a sum of successive corrections,

$$p(x) = p_{\text{guess}}(x) + \sum_{i=1}^{N_{\text{iter}}} \delta p_i(x), \quad (26)$$

in which every  $\delta p_i(x)$  satisfies the equivalent finite difference equation. Since second-order centred finite differences are not able to represent such a high frequency as  $T'_N(x)$ , in the successive corrections the spurious mode is automatically filtered from the solution. Theoretically speaking, one should prove that the space spanned by the finite difference corrections is orthogonal to the space spanned by the spurious modes (3).

The numerical results that have been obtained seem to confirm the effectiveness of such a filtering procedure. In Figure 1 the computed pressure isolines at  $Re = 10$  for the driven regularized cavity (see results sections) using the finite difference preconditioner are given versus those obtained without preconditioning. In the latter the polluting presence of spurious wiggles is dramatically evident.

### 3. SINGLE-BLOCK VALIDATION

The developed single-block algorithm has been validated on different test cases, to be illustrated in the following subsections.

#### 3.1. Driven cavity

The sketch in Figure 2 introduces the first test case. In this problem the flow is driven by a theoretical horizontal motion of the top lid of the cavity such that the horizontal velocity component there is given by  $16x^2(1-x)^2$  and the vertical component is zero. This velocity distribution removes the singularities at the top corners of the standard driven cavity and therefore preserves the high accuracy of the spectral space discretization. The boundary conditions on the other edges are no-slip conditions (zero velocity at the walls).

According to the complexity of the expected flow field, the computations were performed with two different grids:

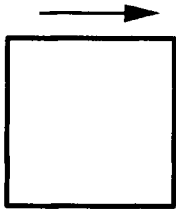
$$U(x) = 16x^2(1-x)^2$$


Figure 2. Driven cavity configuration

Table I. Computed values of component of velocity at cavity centre

Test case	Present	Demaret
$Re = 10$	-0.1653	-0.1653
$Re = 100$	-0.1612	-0.1612
$Re = 1000$	-0.0521	-0.0519

- (i) a  $25 \times 25$  grid for Reynolds numbers up to 5000
- (ii) a  $41 \times 41$  grid at Reynolds number 10,000.

Table I gives a quantitative comparison between the present solutions and those obtained by Demaret<sup>20</sup> for the computed  $x$ -component of velocity at the centre of the cavity.

Table II gives a quantitative comparison of the present results with those obtained by Demaret,<sup>20</sup> Phillips and Roberts<sup>21</sup> and Shen<sup>22</sup> for the positions of primary and secondary vortices at different Reynolds numbers. The first value for each entry refer to the  $x$ -coordinate of the vortex centre ( $0 \leq x \leq 1$ ), while the second value indicates the  $y$ -value ( $0 \leq y \leq 1$ ). Streamline patterns are shown in Figure 3 and 4 at different Reynolds numbers. The results are in good agreement with those obtained by other authors, except at  $Re = 5000$  and 10,000 where a discrepancy concerning the positions of the secondary bottom right vortices is evident. To confirm our results, these two last cases have been rerun with an even finer grid ( $51 \times 51$ ) to demonstrate that the present solution is effectively 'grid-converged'.

### 3.2. Thermally driven cavity

In order to prove the present algorithm robustness with respect to the boundary condition treatment, a thermally driven cavity problem was considered. A square with a side of length  $l$  encloses a fluid initially at temperature  $T_0$ . At time  $t = 0$  the temperature of one wall is raised to  $T_1$ , while the temperature of the opposite wall remains constant and equal to  $T_0$ . The other two walls are insulated (adiabatic walls). This test case is illustrated graphically in Figure 5. The non-dimensionalized variables for the problem are

$$t = \frac{\hat{t}\nu Ra}{l^2}, \quad u = \frac{\hat{u}l}{\nu}, \quad v = \frac{\hat{v}l}{\nu}, \quad T = \frac{\hat{T} - T_0}{T_1 - T_0}, \quad Ra = \frac{g\beta l^3(T_1 - T_0)}{\nu\alpha},$$



Table II Vortex positions

<i>Re</i>	Reference	Primary	Secondary right	Secondary left	Secondary top left
100	Present	0.599, 0.750	0.959, 0.045	0.038, 0.038	—
100	Phillips	0.598, 0.757	0.952, 0.048	0.038, 0.038	—
100	Shen	0.609, 0.750	0.953, 0.047	0.031, 0.031	—
200	Present	0.628, 0.691	0.933, 0.087	0.038, 0.038	—
200	Phillips	0.621, 0.691	0.929, 0.084	0.038, 0.038	—
400	Present	0.565, 0.629	0.897, 0.103	0.038, 0.038	—
400	Phillips	0.573, 0.621	0.902, 0.113	0.048, 0.038	—
400	Shen	0.578, 0.625	0.922, 0.094	0.031, 0.047	—
1000	Present	0.540, 0.574	0.880, 0.114	0.067, 0.067	—
1000	Phillips	0.549, 0.573	0.870, 0.113	0.071, 0.071	—
1000	Shen	0.547, 0.578	0.922, 0.094	0.078, 0.063	—
2000	Present	0.531, 0.548	0.859, 0.107	0.080, 0.097	0.045, 0.898
2000	Phillips	0.525, 0.549	0.854, 0.113	0.084, 0.098	0.038, 0.887
2000	Demaret	0.529, 0.553	0.850, 0.103	0.087, 0.094	0.041, 0.891
2000	Shen	0.531, 0.547	0.922, 0.094	0.078, 0.094	0.031, 0.902
3000	Present	0.522, 0.540	0.842, 0.091	0.082, 0.112	0.062, 0.900
5000	Present	0.517, 0.534	0.814, 0.082	0.081, 0.120	0.080, 0.910
5000	Phillips	0.525, 0.537	0.808, 0.078	0.084, 0.121	0.078, 0.902
5000	Shen	0.516, 0.531	0.922, 0.094	0.094, 0.121	0.078, 0.920
10000	Present	0.514, 0.532	0.786, 0.067	0.065, 0.148	0.094, 0.920
10000	Shen	0.536, 0.531	0.922, 0.094	0.094, 0.094	0.094, 0.092

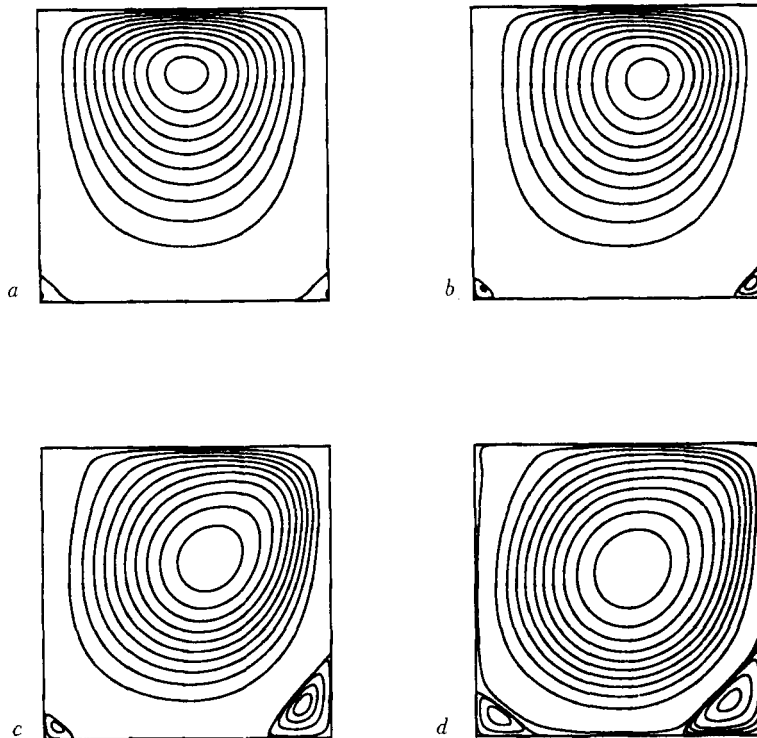


Figure 3. Streamlines contours: a, *Re* = 10; b, *Re* = 100; c, *Re* = 400; d, *Re* = 1000

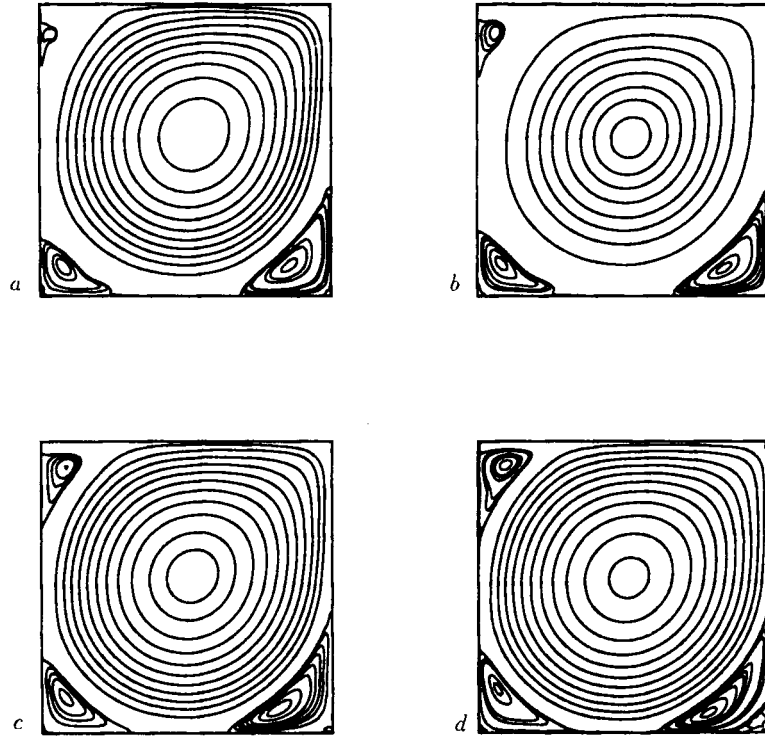


Figure 4. Streamlines contours: a,  $Re = 2000$ ; b,  $Re = 3000$ ; c,  $Re = 5000$ ; d,  $Re = 10,000$

where  $Ra$  is the Rayleigh number,  $g$  is the acceleration due to gravity,  $\beta$  is the thermal expansion coefficient,  $\nu$  is the kinematic viscosity and  $\alpha$  is the thermal diffusivity. The governing equations according to the Boussinesq approximation are

$$\begin{aligned} \frac{\partial u}{\partial t} + u \frac{\partial u}{\partial x} + v \frac{\partial u}{\partial y} &= -\frac{\partial p}{\partial x} + \frac{Pr}{\sqrt{(Ra)}} \Delta u, \\ \frac{\partial v}{\partial t} + u \frac{\partial v}{\partial x} + v \frac{\partial v}{\partial y} &= -\frac{\partial p}{\partial y} + \frac{Pr}{\sqrt{(Ra)}} \Delta v + TPr, \\ \frac{\partial u}{\partial x} + \frac{\partial v}{\partial y} &= 0, \\ \frac{\partial T}{\partial t} + u \frac{\partial T}{\partial x} + v \frac{\partial T}{\partial y} &= \frac{1}{\sqrt{(Ra)}} \Delta T, \end{aligned}$$

where  $Pr$  is the Prandtl number ( $Pr = C_p \mu / k$ ). The initial conditions are

$$\begin{aligned} u = v = 0 & \quad \text{for } 0 \leq x \leq 1, 0 \leq y \leq 1, \\ T = 0 & \quad \text{for } 0 \leq x \leq 1, 0 \leq y \leq 1. \end{aligned}$$

Two different boundary condition arrangements were considered.

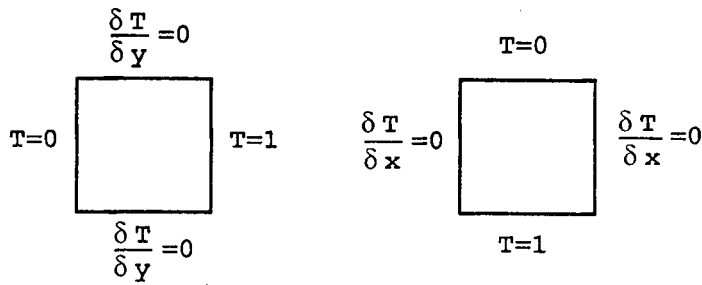


Figure 5. Thermally driven cavity configurations

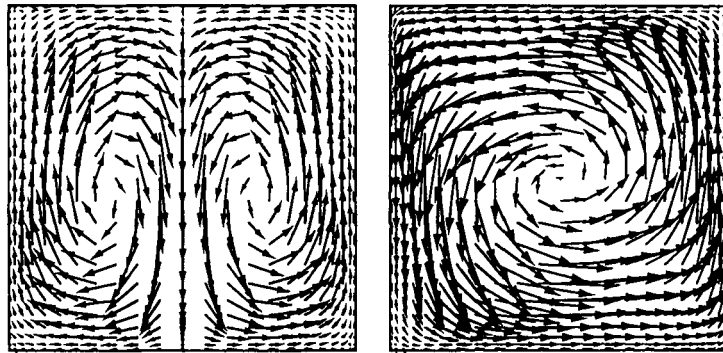


Figure 6. Velocity vector fields

1. Horizontal adiabatic walls (Figure 5, left):

$$\begin{aligned}
 t > 0, \quad u = v = 0 \quad \text{on } x = 0, y = 0, 1, \\
 T = 0, \quad x = 0, \\
 T = 1, \quad x = 1, \\
 \partial T / \partial y = 0, \quad y = 0, 1.
 \end{aligned}$$

2. Vertical adiabatic walls (Figure 5, right):

$$\begin{aligned}
 t > 0, \quad u = v = 0 \quad \text{on } x = 0, 1, y = 0, \\
 T = 1, \quad y = 0, \\
 T = 0, \quad y = 1, \\
 \partial T / \partial x = 0, \quad x = 0, 1.
 \end{aligned}$$

The computed velocity fields induced by the imposed temperature gradients are shown in Figure 6. Table III gives a quantitative comparison between the present results and those obtained by Hwar *et al.*<sup>23</sup> for the horizontal adiabatic walls test case at  $Ra = 10^4$  and  $Pr = 0.71$ . Here we give the temperature profiles going from right to left at the centreline of the cavity (i.e.

Table III Temperature profile

x	Present	Hwar
0.9830	0.959	0.959
0.9331	0.836	0.840
0.8536	0.673	0.674
0.7500	0.542	0.542
0.6294	0.495	0.495
0.5000	0.499	0.500
0.3706	0.504	0.505
0.2500	0.458	0.459
0.1465	0.326	0.326
0.0670	0.160	0.160
0.0171	0.041	0.041

$y = 0.5$ ). In general there is almost exact agreement between our results and those computed by Hwar *et al.*

### 3.3. Unsteady driven cavity

To validate the developed code for unsteady calculations, we considered once more the regularized driven cavity flow at higher Reynolds numbers.

The choice of the test case stems from the calculations of Shen<sup>22</sup> on the same configuration. He found a persistent oscillation when increasing the Reynolds number up to a critical value of 10,500. The same author has also observed that for  $Re \geq 15,000$  the dynamical behaviour of the flow patterns was losing time periodicity. These observations led the author to conjecture that a Hopf bifurcation might occur in the critical range  $10,500 \leq Re \leq 15,000$ .

For our computations we selected the first critical Reynolds numbers (i.e.  $Re = 10,500$ ).

The grid used for this test case was a  $41 \times 41$  one. A finer grid of  $51 \times 51$  has been employed to check that the obtained results were 'grid-converged'.

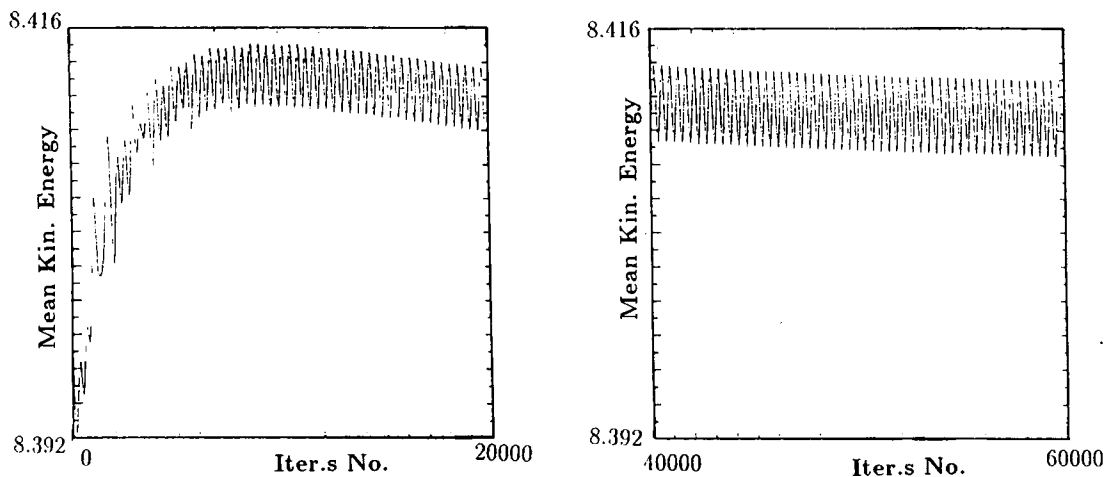


Figure 7. Time behaviour of mean kinetic energy

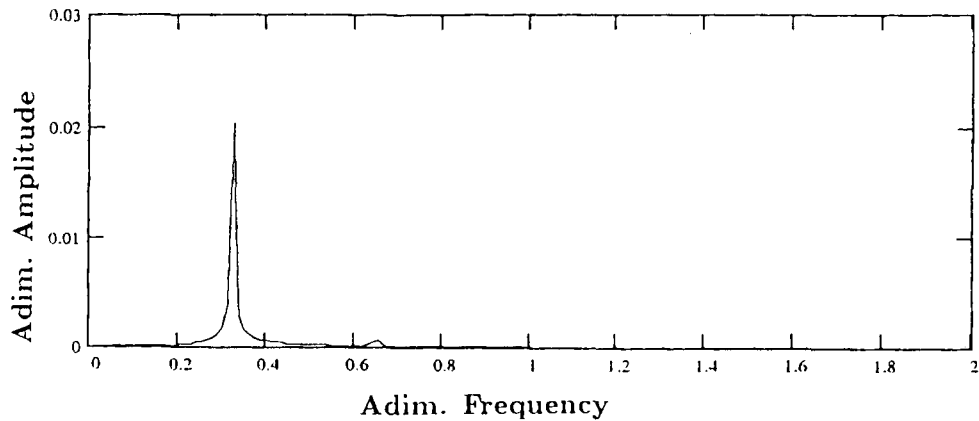
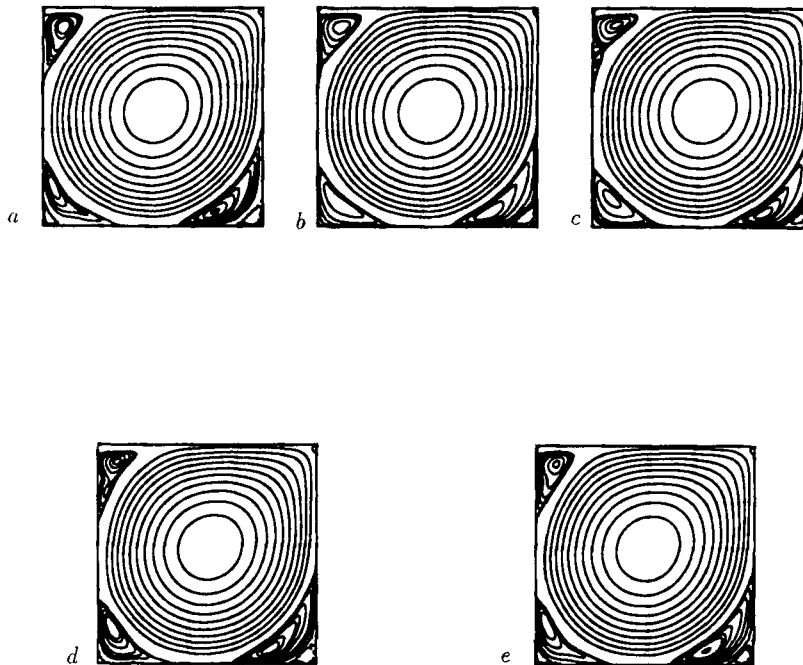


Figure 8. Spectral analysis of kinetic energy

Figure 9. Streamline contours: a,  $t = T$ ; b,  $t = T + T/4$ ; c,  $t = T + T/2$ ; d,  $t = T + 3T/4$ ; e,  $t = 2T$  ( $T$ , period)

In agreement with what has been observed by Shen,<sup>22</sup> also in our case at  $Re = 10,500$  no steady solution is found; instead, after a long transient the flow finally becomes periodic in time.

In Figure 7 we show the time behaviour of the mean kinetic energy  $\sqrt{\sum_i (u_i^2 + v_i^2)}$ , which reaches an asymptotic behaviour only after quite a long integration time (on the  $x$ -axis each unit corresponds to 10 time steps,  $\sim 0.08$  time units).

A spectral analysis of both the  $x$ -component of velocity and the kinetic energy at a fixed point ( $x = 0.038$ ,  $y = 0.990$ ) shows a frequency peak (see Figure 8) which reveals that a periodic motion is taking place with a frequency of about 0.33 frequency units. Finally, in Figure 9 we present

five streamline patterns extracted within one full time period to show the quite complex flow behaviour (vortex breakdown, appearance and disappearance of tertiary vortices, etc.).

#### 4. MULTIDOMAIN ALGORITHM

In the previous sections we have concentrated on the application of pseudospectral methods for the Navier–Stokes equations on the standard Chebyshev square. There have been a number of recent developments on the use of spectral techniques in more general geometries.<sup>24,25</sup>

The basic idea underlying the multidomain approach for spectral methods relies on partitioning the given geometry into union of elementary squares. The approximation is spectral if increased accuracy is obtained by increasing the order of the approximation in a fixed number of subdomains rather than resorting to a further partitioning. Apart from the evident advantages of being able to deal with complex geometries, other advantages might be achieved using domain decomposition techniques: better distribution of collocation points, which improves the resolution; better conditioning of the associated algebraic problems (due to a less extreme ratio of the largest to the smallest grid spacings); finally, evident advantages in the implementation of spectral codes on parallel machines.

A crucial aspect of any domain decomposition method is the manner in which solutions on contiguous domains are matched. In the following we will concentrate only on ‘patching’ methods that have been selected in the frame of the present work.

Patching methods take a pointwise view of the differential equation. If the equations have order  $d$ , then at the interface of contiguous domains the solution and all its derivatives of order up to  $d - 1$  must be continuous.<sup>26</sup> Normally, elliptic problems require implicit methods for the interface treatment. The matrices which represent the global algebraic system have a block structure due to the domain decomposition, and only adjacent subdomains (or blocks) are coupled. One obvious strategy would be a direct Gauss elimination, but this proves to be expensive in terms of storage and CPU time. Another approach which avoids the solution of a global system is based on an iterative procedure amongst subdomains, yielding a sequence of a single-domain boundary value problem. One simply iterates between adjacent subdomains by imposing alternately the continuity of the solution and the continuity of the normal derivatives. At the limit of the convergence process, continuity conditions at the interfaces are therefore satisfied.<sup>27</sup>

In the next subsection the particular iterative method that has been used in the present work in the framework of the incompressible Navier–Stokes equations will be illustrated.

##### 4.1. The iterative method

Many iterative procedures have been proposed in the last five years.<sup>28,29</sup> We selected the one proposed by Funaro *et al.*<sup>9</sup> In such a procedure, at each iteration a relaxation is accomplished at the subdomain interfaces. The authors also provide an appropriate strategy for the automatic selection of the relaxation parameter to be used at each iteration. To illustrate the procedure, we confine ourselves to a Helmholtz problem:

$$-\Delta u + \mu u = f \quad \text{on } \Omega \quad \text{with } u = 0 \quad \text{on } \partial\Omega. \quad (27)$$

Defining  $\Omega = (-a, b) \times (-1, 1)$  decomposed into the subsets  $\Omega_1 = (-a, 0) \times (-1, 1)$  and  $\Omega_2 = (0, b) \times (-1, 1)$ , we denote by  $\partial\Omega$  the boundary of  $\Omega$  and by  $\Gamma = 0 \times (-1, 1)$  the interface between  $\Omega_1$  and  $\Omega_2$  (see Figure 10). The iterative procedure goes as follows:

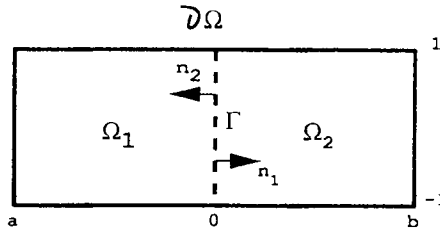


Figure 10. Partitioning of domain

$$-\Delta v^{(n)} + \mu v^{(n)} = f \quad \text{on } \Omega_1, \tag{28}$$

$$v^{(n)} = 0 \quad \text{on } \partial\Omega_1, \tag{29}$$

$$v^{(n)} = \lambda_n \quad \text{on } \Gamma \tag{30}$$

and

$$-\Delta w^{(n)} + \mu w^{(n)} = f \quad \text{on } \Omega_2, \tag{31}$$

$$w^{(n)} = 0 \quad \text{on } \partial\Omega_2, \tag{32}$$

$$\partial w^{(n)} / \partial x = \partial v^{(n)} / \partial x \quad \text{on } \Gamma, \tag{33}$$

where

$$\lambda_{n+1} = \theta w^{(n)} + (1 - \theta)\lambda_n \quad \text{on } \Gamma \quad \text{for } n \geq 1 \tag{34}$$

and  $\theta \in ]0, 1]$  is a relaxation parameter. If  $\theta = 1$ , we do not have relaxation and under this condition convergence is obtained if and only if  $a > b$ .<sup>9</sup> An iterative relaxation scheme of this form was formerly proposed by Zanolli.<sup>30</sup> If the sequences  $v^{(n)}$  and  $w^{(n)}$  converge, their limits are necessarily the solutions  $v$  and  $w$  to (27).

If we consider the collocated versions of (28) and (31), it is possible to introduce a dynamical procedure to determine the relaxation parameter  $\theta$ . In fact, if we define the error functions at the  $N$  nodes at the interface as

$$e_{v,N}^n = v_N^n - v_N^{n-1} \in P_N^1 \quad \text{and} \quad e_{w,N}^n = w_N^n - w_N^{n-1} \in P_N^2 \quad \text{for } n \geq 2, \tag{35}$$

where the superscript  $n$  refers to the  $n$ th iteration, it is possible to select the value of  $\theta$  at iteration  $n$  as

$$\theta_n = \frac{(e_{v,N}^n, e_{v,N}^n - e_{w,N}^n)}{\|e_{v,N}^n - e_{w,N}^n\|^2}, \quad n \geq 2, \tag{36}$$

whose associated norms is  $\|u\| = \sqrt{(u, u)}$ . For the formal convergence proofs and more precise details the reader is referred to the original paper.<sup>9</sup>

#### 4.2. Application to Navier–Stokes equations

As already mentioned, when the incompressible Navier–Stokes equations are solved by means of a projection method, with the diffusive part treated in an implicit fashion, the time-stepping procedure consists of a cascade of two Helmholtz problems for the predicted velocity components

and a Poisson equation for the pressure. If one tackles each single differential problem with the iterative procedure by subdomains described in the previous subsection, at the end of each time step the solution is equivalent to the one hypothetically achievable by solving the whole domain at once. Let us develop this basic idea. We start by solving two Helmholtz problems for  $\hat{u}$  and  $\hat{v}$  by imposing iteratively the continuity of the function and of its normal derivatives for both the predicted velocity components. When convergence of the iterative procedure by subdomains is attained, the two variables will  $\in C^1(\Omega)$ . The continuity of  $\text{div}(\mathbf{u})$  on the whole domain is therefore guaranteed. In other words we obtain a right-hand side for the Poisson problem (the pressure equation) that is of class  $\in C^0(\Omega)$ . This condition ensures that the pressure  $p \in C^1(\Omega)$ . Under such a condition the iterative procedure (28, 31) becomes applicable.<sup>9</sup> In particular, when the iterative procedure applied to the Poisson equation converges, we will recover the pressure  $\in C^1$  at the interfaces as well. Finally let us consider the projection step

$$\frac{\mathbf{u}^{n+1} - \hat{\mathbf{u}}}{\Delta t} + \frac{1}{2}\nabla(p^{n+1} - p^n) = 0. \quad (37)$$

It is evident that the final value of the velocity ( $\mathbf{u}^{(n+1)}$ ) will  $\in C^1(\Omega_i)$  at the interior points. On the interfaces the function will be continuous, since it is the sum of continuous functions, and its first derivative will match on the interface with a deviation  $\mathcal{O}(\Delta t^2)$ . In particular the mismatch of the first derivative at the interface is quantified in the normal direction by

$$\Delta t \left( \frac{\partial^2(p_i^{n+1} - p_i^n)}{\partial n^2} - \frac{\partial^2(p_{i+1}^{n+1} - p_{i+1}^n)}{\partial n^2} \right) \quad (38)$$

and in the tangential direction by

$$\Delta t \left( \frac{\partial^2(p_i^{n+1} - p_i^n)}{\partial n \partial \tau} - \frac{\partial^2(p_{i+1}^{n+1} - p_{i+1}^n)}{\partial n \partial \tau} \right). \quad (39)$$

Both the errors correspond to the splitting errors at the boundaries typical of any projection method. In particular the mismatch on the normal derivative leads to an error that is analogous to the one associated with the slip error at a solid boundary, while the mismatch in the tangential direction is equivalent to the ‘permeability’ error at inflow–outflow boundaries. Of course for stationary problems at steady state (i.e. convergence) the errors (38) and (39) at the interface drop to zero and the continuity of both the velocities and their first derivatives is ensured, leading to the correct solution on the whole domain.

For unsteady problems the errors at the interface are of the same order as those at the boundaries and for this reason the present method may also be used for unsteady calculations.

## 5. MULTIDOMAIN VALIDATION

Laminar and turbulent flow in a pipe or channel expansion is a complex flow situation often used as a test for numerical and experimental techniques. We choose the problem of the flow in an asymmetric channel expansion to demonstrate the viability of the present multidomain techniques.

The channel configuration is shown in Figure 11. It is assumed that the channel length prior to the step is sufficiently long to allow the imposition of a parabolic profile at the inlet. The Navier–Stokes equations are non-dimensionalized with respect to the inlet channel half-width  $h$  and the maximum velocity at the inlet ( $Re = U_{\max} h/\nu$ ).



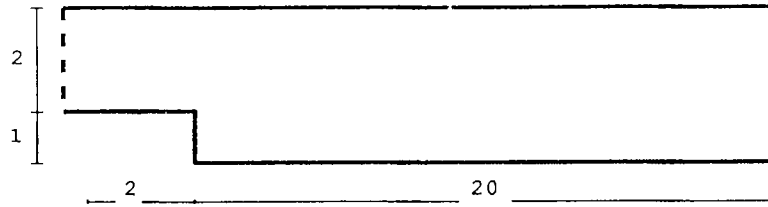


Figure 11. Geometry of backward-facing step



Figure 12. Grid configuration

The step height is taken to be the same as the channel half-width, while the non-dimensional length of the channel following the expansion is taken to be sufficiently long ( $\sim 20$ ) so as not to affect the phenomena of interest. For the computation we restricted ourselves to laminar, moderate Reynolds numbers (i.e.  $\sim 100$ ). There are several criteria on which comparisons can be made with previous numerical work and experiments: the position of the centre of the separated vortex; the point of the flow reattachment; the streamwise velocity profile at various points downstream.

For the computation we partitioned the domain into three subdomains of  $15 \times 15$  nodes properly mapped according to the height and length of each subelement. The grid is shown in Figure 12.

In Figure 13, we show the streamline contours at  $Re = 109$ . It is seen that the reattachment length is 5.1, which is in good agreement with both the experimental value<sup>5</sup> and values obtained with other spectral computations.<sup>31</sup>



Figure 13. Streamline contours

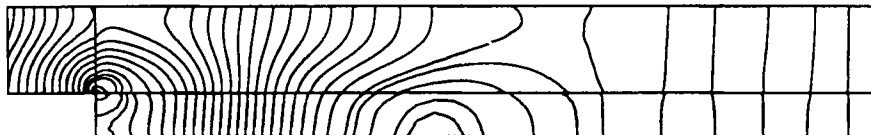


Figure 14. Isopressure lines

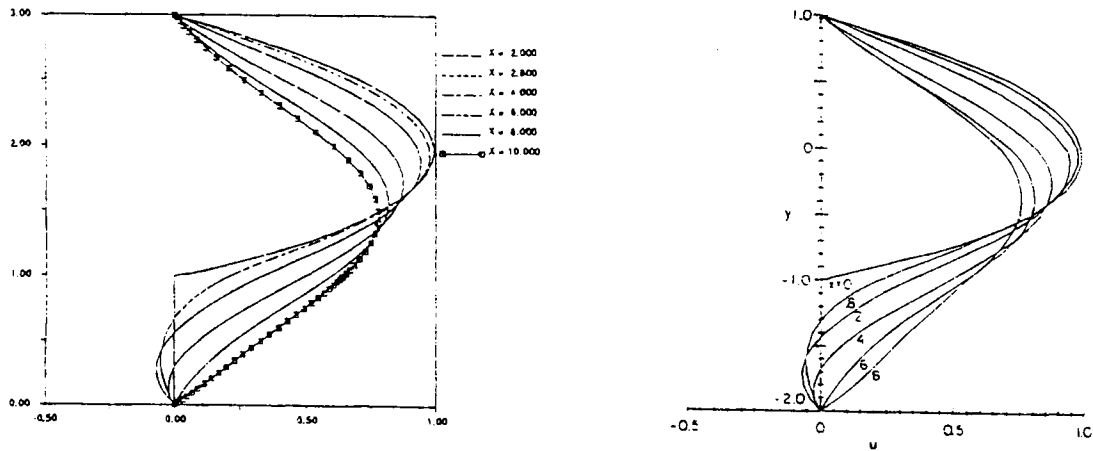


Figure 15. Streamwise velocity profiles: left, present; right, Patera<sup>5</sup>

In Figure 14 we show the isopressure lines at the same Reynolds number. In Figure 15 we compare the streamwise velocity profiles at various points downstream with those obtained by Patera with a 'spectral element' code.<sup>5</sup>

## 6. CONCLUSIONS

The two-dimensional incompressible Navier–Stokes equations have been solved by a pseudo-spectral Chebyshev expansion method using a second-order time-splitting scheme (projection method).

The first task has been the design of an efficient 'single-block' algorithm to be used as computational kernel for a multidomain solver.

The mentioned scheme requires the solution of two Helmholtz problems and a Poisson problem at each time step. Each elliptic scalar problem has been solved by means of an iterative procedure preconditioned by centred finite differences. In particular, the above-mentioned iterative procedure applied to the inversion of the Poisson problem for the pressure behaves like a 'low-passband' filter, removing spurious pressure modes from the calculation without any loss of accuracy.

Once the 'single-block' solver has been validated, a multidomain algorithm has been designed by taking advantage of the algorithm structure of the monodomain one. More precisely, an iterative procedure 'by subdomains' has been applied to each scalar equation arising after the application of the time-splitting scheme.

The devised procedures have been tested and validated for a number of test cases both for the 'single-block' solver and for its multidomain configuration.

The major limitations of the present method as presented in this paper are due to the inefficiency of the multidomain algorithm when dealing with 'internal corners' and the restrictions on the allowed time step when solving high-Reynolds-number problems. These deficiencies are currently being addressed, the former by the implementation of a novel 'iteration by subdomains' algorithm and the latter by the introduction of an implicit procedure for the treatment of the advective terms.

## ACKNOWLEDGEMENT

The above text presents research results of the Belgian Incentive Program *Information Technology—Computer Science of the Future*, initiated by the Belgian State, Prime Minister's Service, Science Policy Office. The scientific responsibility is assumed by its authors.

## REFERENCES

1. S. A. Orszag, 'Spectral methods for problems in complex geometries', *J. Comput. Phys.*, **37**, 70–92 (1980).
2. T. F. Chan, R. Glowinski, J. Periaux and O. B. Widlund (eds), *Proc. Second Int. Symp. on Domain Decomposition Methods*, Los Angeles, CA, January 1988, SIAM, Philadelphia, PA, 1988.
3. T. F. Chan, R. Glowinski, J. Periaux and O. B. Widlund (eds), *Proc. Third Int. Symp. on Domain Decomposition Methods*, Houston, TX, March 1989, SIAM, Philadelphia, PA, 1989.
4. P. R. Eisemann and G. Erlebacher, 'Grid generation for the solution of partial differential equations', *NASA CR-178365*, 1987; also *ICASE Rep. 85-57*, 1985 (unpublished).
5. A. T. Patera, 'A spectral element method for fluid dynamics: laminar flow in a channel expansion', *J. Comput. Phys.*, **54**, 468–488 (1984).
6. K. Z. Korczak and A. T. Patera, 'Isoparametric spectral element method for the solution of the Navier-Stokes equations in complex geometries', *J. Comput. Phys.*, **62**, 361–382 (1986).
7. B. Metivet, *Thèse de Doctorat d'Etat*, Université Pierre et Marie Curie, Paris 6, 1987 (unpublished).
8. J. Van Kan, 'A second order accurate pressure-correction scheme for viscous incompressible flow', *J. Sci. Stat. Comput.*, **7**, 870–891 (1986).
9. D. Funaro, A. Quarteroni and P. Zanolli, 'An iterative procedure with interface relaxation for domain decomposition methods', *SIAM J. Numer. Anal.*, **25**, 1213–1236 (1988).
10. A. Pinelli, A. Vacca, C. Benocci and M. Deville, 'A Chebyshev collocation algorithm for the solution of incompressible 2-D Navier–Stokes equations', In C. Taylor (ed.), *Proc. 8th Int. Conf. on Numerical Methods in Laminar and Turbulent Flows*, Swansea, July 1993, Pineridge, Swansea, 1993.
11. Y. Maday, 'Introduction to spectral methods', *Von Karman Institute Lecture Series 1993–04*, Rhode-St.-Genèse, 1993.
12. A. Chorin and J. Marsden, *A Mathematical Introduction to Fluid Mechanics*, Springer, New York, 1979.
13. R. Temam, *Navier–Stokes Equations*, North-Holland, Amsterdam, 1977.
14. T. Zang, C. Streett and M. Hussaini, 'Spectral methods for C.F.D.', *ICASE Rep. 89–13*, 1989.
15. C. Canuto, M. Y. Hussaini, A. Quarteroni and T. A. Zang, *Spectral Methods in Fluid Dynamics*, Springer, New York, 1988.
16. P. Haldenwang, G. Labrosse, S. Abboudi and M. Deville, 'Chebyshev 3-D spectral and 2-D pseudo-spectral solver for the Helmholtz equations', *J. Comput. Phys.*, **55**, 115–128 (1984).
17. G. H. Golub and C. F. Van Loan, *Matrix Computations*. Johns Hopkins University Press, Baltimore, MD, 1989.
18. S. Eisenstat, H. Elman and M. Shultz, 'Variational iterative methods for non-symmetric systems of linear equations', *SIAM J. Numer. Anal.*, **20**, 345–357 (1983).
19. F. Brezzi, 'On the existence, uniqueness and approximation of saddle point problems arising from Lagrange multipliers', *RAIRO Numer. Anal.*, **8**, 129–151 (1974).
20. P. Demaret, *Ph.D. Thesis*, Université Catholique de Louvain, 1989.
21. T. Phillips and G. Roberts, 'The treatments of spurious pressure modes in spectral incompressible flow calculations', *J. Comput. Phys.*, **105**, 150–164 (1993).
22. J. Shen, 'The Hopf bifurcation on the unsteady regularized driven cavity flow', *J. Comput. Phys.*, **95**, 228–245 (1991).
23. C. Hwar, T. Taylor and R. Hirsch, 'Pseudo-spectral methods for the solution of the incompressible Navier–Stokes equations', *Comput. Fluids*, **15**, 195–214 (1987).
24. E. Ronquist and A. T. Patera, 'A Legendre spectral element method for the incompressible Navier-Stokes equations', *Proc. 7th GAMM Conf. on Numerical Methods in Fluid Mechanics*, Vieweg, Braunschweig, 1988.
25. E. Ronquist, 'Spectral elements methods for fluid dynamics', *Von Karman Institute Lecture Series 1991–01*, Rhode-St.-Genèse, 1991.
26. J. L. Lions and E. Magenes, *Nonhomogeneous Boundary Value Problems and Applications*, Vol. 1, Springer, Berlin, 1972.
27. L. Marini and A. Quarteroni, 'A relaxation procedure for domain decomposition methods using finite elements', *Numer. Math.*, **55**, 575–598 (1989).
28. B. Metivet and Y. Morchoisne, 'Multi-domain spectral technique for viscous flow calculation', *Proc. 4th GAMM Conf. on Numerical Methods in Fluid Mechanics*, Vieweg, Braunschweig, 1982.
29. M. Macaraeg and C. Streett, 'Improvements in spectral collocation through a multiple domain technique', *App. Numer. Math.*, **2**, 95–108 (1986).
30. A. Quarteroni and A. Valli, 'Theory and application of Steklov–Poincaré operators for boundary value problems: the heterogeneous operators case', *University of Minnesota Supercomputer Institute Res. Rep. UMSI 90-232*, 1990.
31. B. Armaly, F. Durst, J. Pereira and B. Schonung, 'Experimental and theoretical investigation of backward facing step flow', *J. Fluid. Mech.*, **127**, 473–496 (1983).